Low-power photothermal self-oscillation of bimetallic nanowires
SUPPLEMENTARY INFORMATION

Roberto De Alba,[1] T. S. Abhilash,[1] Richard H. Rand,[2,3] Harold G. Craighead,[4] and Jeevak M. Parpia[1]

[1]*Department of Physics, Cornell University, Ithaca NY, USA*
[2]*Department of Mathematics, Cornell University, Ithaca NY, USA*
[3]*Sibley School of Mechanical and Aerospace Engineering, Cornell University, Ithaca NY, USA*
[4]*School of Applied and Engineering Physics, Cornell University, Ithaca NY, USA*

CONTENTS

S1. PERTURBATION THEORY FOR PHOTOTHERMAL SELF-OSCILLATION

The governing equations of motion are:

$$\ddot{z} + \gamma\dot{z} + \omega_{0i}^2(1 + CT)(z - DT) = 0 \tag{S1}$$

$$\dot{T} + \frac{1}{\tau}T = APg(z) \tag{S2}$$

$$g(z) = \alpha - \beta\sin\left(\frac{4\pi(z+\phi)}{\lambda}\right) \tag{S3}$$

Eqs. S1 & S2 have the static solution $z_0 = \tau DAPg(z_0)$ and $T_0 = z_0/D$. We can define a new coordinate system as deviations from this equilibrium $x = z - z_0$ and $u = T - T_0$, which leads to:

$$\ddot{x} + \gamma\dot{x} + \omega_{0i}^2(1 + CT_0 + Cu)(x - Du) = 0 \tag{S4}$$

$$\dot{u} + \frac{1}{\tau}u = -\frac{1}{\tau}T_0 + APg(x + z_0) \tag{S5}$$

$$g(x + z_0) = \alpha - \beta\sin\left(\frac{4\pi(x + z_0 + \phi)}{\lambda}\right) \tag{S6}$$

where we have introduced $x_0 = \phi - z_0$. For convenience we now rescale our units of time and displacement such that the resonant frequency $\omega_{0i} = 1$ and laser wavelength $\lambda = 1$:

$$\ddot{x} + \frac{1}{Q}\dot{x} + (1 + CT_0 + Cu)(x - D'u) = 0 \tag{S7}$$

$$\dot{u} + \frac{1}{\tau'}u = -\frac{1}{\tau'}T_0 + A'Pg(x + z_0) \tag{S8}$$

$$g(x + z_0) = \alpha - \beta\sin\left(4\pi(x + z_0 + \phi)\right). \tag{S9}$$

Here the quantities x, z_0, ϕ are now expressed in units of λ and we have introduced the quality factor $Q = \omega_{0i}/\gamma$. Furthermore, we have defined $D' = D/\lambda$, $\tau' = \tau\omega_{0i}$, and $A' = A/\omega_{0i}$. Hereafter we will work exclusively with these rescaled parameters, and for brevity we will not write the primes.

In performing the perturbation theory, we will be required to approximate $g(x + z_0)$ by a polynomial. We choose to expand $g(x + z_0)$ in a Taylor series about $x + z_0 = -\phi$ so that the coefficients of our series are independent of ϕ. We will truncate this series at $N + 1$ terms, and refer to the truncated series as $h(x) \approx g(x + z_0)$:

$$h(x) = \sum_{n=0}^{N} \frac{g^{(n)}(-\phi)}{n!}(x + z_0 + \phi)^n = \sum_{n=0}^{N} k_n(x + z_0 + \phi)^n \tag{S10}$$

where $g^{(n)}(-\phi)$ denotes the nth derivative of $g(x + z_0)$ evaluated at $x + z_0 = -\phi$. Note that if $N \to \infty$ we have $h(x) = g(x + z_0)$. The first few coefficients k_n are given by:

$$\begin{aligned}
k_0 &= \alpha \\
k_1 &= -4\pi\beta \\
k_3 &= \frac{32}{3}\pi^3\beta \\
k_5 &= -\frac{128}{15}\pi^5\beta \\
k_7 &= \frac{1024}{315}\pi^7\beta \\
k_n &= 0, \;\; \text{even } n > 0
\end{aligned} \tag{S11}$$

Thus, finally, we will seek a solution to the coupled differential equations:

$$\ddot{x} + \frac{1}{Q}\dot{x} + (1 + CT_0 + Cu)(x - Du) = 0 \tag{S12}$$

$$\dot{u} + \frac{1}{\tau}u = -\frac{1}{\tau}T_0 + APh(x) \tag{S13}$$

We will solve Eqs. S12 & S13 via the Poincaré-Lindstedt perturbation method. To do this, we must scale $1/Q, Cu$, and Du by a small dimensionless parameter $\epsilon \ll 1$. This will yield solutions for $x(t)$ and $u(t)$ that are power series in ϵ: $x = x_1 + x_2\epsilon + x_3\epsilon^2 + \cdots$ and $u = u_1 + u_2\epsilon + u_3\epsilon^2 + \cdots$. In order to perturbatively solve for the oscillation frequency $\omega = \omega_1 + \omega_2\epsilon + \omega_3\epsilon^2 + \cdots$ we once more scale the time dimension by ω. This leads to the coupled system:

$$\omega^2\ddot{x} + \frac{\epsilon\omega}{Q}\dot{x} + (1 + CT_0 + \epsilon Cu)(x - \epsilon Du) = 0 \tag{S14}$$

$$\omega\dot{u} + \frac{1}{\tau}u = -\frac{1}{\tau}T_0 + APh(x) \tag{S15}$$

Setting $\epsilon = 0$ gives us the lowest order of the perturbation:

$$\omega_1^2\ddot{x}_1 + (1 + CT_0)x_1 = 0 \tag{S16}$$

$$\omega_1\dot{u}_1 + \frac{1}{\tau}u_1 = -\frac{1}{\tau}T_0 + APh(x_1) \tag{S17}$$

Choosing $\omega_1^2 = 1 + CT_0$ in Eq. S16 results in the solution $x_1 = R\cos t$. This solution is now substituted into Eq. S17 to solve for u_1. Because $h(x_1)$ is a polynomial in x_1, this leads to:

$$\omega_1\dot{u}_1 + \frac{1}{\tau}u_1 = V_0 + \sum_{n=1}^{N} V_n \cos nt \tag{S18}$$

where V_0 and V_n are constant coefficients that depend on T_0, R, and the details of $h(x_1)$. We will derive these coefficients on the next page, but for now we proceed assuming they are known.

Solving Eq. S18, the steady-state solution (i.e. neglecting transient components) for u_1 is:

$$u_1(t) = \tau V_0 + \sum_{n=1}^{N} \frac{\tau V_n}{1 + n^2\omega_1^2\tau^2}(\cos nt + n\omega_1\tau \sin nt) \tag{S19}$$

Thus the time-averaged value of u (to order ϵ^0 in perturbation theory) increases by an amount τV_0 during oscillation.

We now proceed to order ϵ^1 of perturbation theory by substituting $x = x_1 + \epsilon x_2$, $u = u_1 + \epsilon u_2$ and $\omega = \omega_1 + \epsilon\omega_2$ into Eq. S14 and neglecting terms of order ϵ^2 and higher:

$$\epsilon\omega_1^2\ddot{x}_2 + \epsilon\omega_1^2 x_2 + 2\epsilon\omega_1\omega_2\ddot{x}_1 + \frac{\epsilon\omega_1}{Q}\dot{x}_1 - \epsilon\omega_1^2 Du_1 + \epsilon Cu_1 x_1 = 0 \tag{S20}$$

Rearranging terms, this equation can be written in the more familiar form:

$$\ddot{x}_2 + x_2 = -\frac{2\omega_2}{\omega_1}\ddot{x}_1 - \frac{1}{\omega_1 Q}\dot{x}_1 + Du_1 - \frac{C}{\omega_1^2}u_1 x_1 \tag{S21}$$

Thus x_2 represents a simple harmonic oscillator with forcing terms given by the right hand side of Eq. S21. In order for x_2 not to grow without bound, secular terms must be removed. In other words the forcing terms at frequency $\omega = 1$ must vanish. Thus we proceed by substituting $x_1 = R\cos t$ and Eq. S19 for u_1, collecting terms proportional to $\cos t$ and $\sin t$, and equating them to zero. Collecting $\sin t$ terms in Eq. S21 leads to

$$\frac{\omega_1^2 DV_1}{1 + \omega_1^2\tau^2} - \frac{CRV_2}{1 + 4\omega_1^2\tau^2} + \frac{R}{\tau^2 Q} = 0 \tag{S22}$$

which can be solved for R, bearing in mind that the coefficients V_1 and V_2 are dependent on R. Collecting $\cos t$ terms in Eq. S21 gives

$$\frac{2\tau\omega_1^2 DV_1}{1 + \omega_1^2\tau^2} - \frac{\tau CRV_2}{1 + 4\omega_1^2\tau^2} + 4R\omega_1\omega_2 - 2\tau CRV_0 = 0 \tag{S23}$$

which can be solved for ω_2 once R is known.

According to Eq. S22, the oscillation amplitude R is determined by the coefficients V_1 and V_2, which are the forcing terms for u at frequency ω and 2ω in Eq. S18. Moreover, the average temperature change is determined by V_0. We will now proceed to calculate these terms based on $h(x)$ in Eq. S17.

Deriving V_0, V_1, and V_2 is most easily done if we first rewrite $h(x)$ as a series in x rather than $x + z_0 + \phi$. Thus we have

$$h(x) = \sum_{n=0}^{N} \frac{h_0^{(n)}}{n!} x^n \tag{S24}$$

where $h_0^{(n)}$ is the nth derivative of $h(x)$ evaluated at $x = 0$. Note that this Taylor series terminates at order x^N because $h(x)$ is by definition an Nth order polynomial (see Eq. S10). If we take $h(x)$ to be 7th order, as is done in the main text, then the derivatives $h_0^{(n)}$ are related to the factors k_n in Eq. S10 by:

$$
\begin{aligned}
h_0^{(0)} &= k_0 + k_1 x_0 + k_3 x_0^3 + k_5 x_0^5 + k_7 x_0^7 \\
h_0^{(1)} &= k_1 + 3k_3 x_0^2 + 5k_5 x_0^4 + 7k_7 x_0^6 \\
h_0^{(2)} &= 6k_3 x_0 + 20k_5 x_0^3 + 42k_7 x_0^5 \\
h_0^{(3)} &= 6k_3 + 60k_5 x_0^2 + 210k_7 x_0^4 \\
h_0^{(4)} &= 120k_5 x_0 + 840k_7 x_0^3 \\
h_0^{(5)} &= 120k_5 + 2520k_7 x_0^2 \\
h_0^{(6)} &= 5040k_7 x_0 \\
h_0^{(7)} &= 5040k_7
\end{aligned}
\tag{S25}
$$

where we have defined $x_0 = z_0 + \phi$. Equating the right hand sides of Eqs. S17 & S18 then gives:

$$V_0 + \sum_{m=1}^{N} V_m \cos mt = -\frac{1}{\tau} T_0 + AP \sum_{n=0}^{N} \frac{h_0^{(n)}}{n!} x_1^n \tag{S26}$$

In order to calculate V_0, V_1, and V_2 we now substitute $x_1 = R \cos t$ and invoke the power formulas for cosines

even n : $$\cos^n t = \frac{1}{2^n} \binom{n}{n/2} + \frac{1}{2^{n-1}} \sum_{k=0}^{(n/2)-1} \binom{n}{k} \cos[(n-2k)t] \tag{S27}$$

odd n : $$\cos^n t = \frac{1}{2^{n-1}} \sum_{k=0}^{(n-1)/2} \binom{n}{k} \cos[(n-2k)t] \tag{S28}$$

where $\binom{a}{b} = a!/(b!(a-b)!)$ is a binomial coefficient. For even n, the constant term arising from $\cos^n t$ is simply $(1/2^n)\binom{n}{n/2}$. Furthermore, because only $\cos^n t$ with even n will lead to $\cos mt$ with even m, the V_0 in Eq. S26 is

$$
\begin{aligned}
V_0 &= -\frac{1}{\tau} T_0 + AP \sum_{n=0,2,4,\ldots}^{N} \frac{h_0^{(n)}}{n!} \left(\frac{R}{2}\right)^n \frac{n!}{(n/2)!(n/2)!} \\
&= -\frac{1}{\tau} T_0 + AP \sum_{m=0}^{M_0} \frac{h_0^{(2m)}}{(m!)^2} \left(\frac{R}{2}\right)^{2m}
\end{aligned}
\tag{S29}
$$

where $M_0 = \text{floor}(N/2)$. The value of V_0 can similarly be found by substituting Eq. S28 into Eq. S26 with $n - 2k = 1$. Only odd $n \geq 1$ contribute to this sum. This gives

$$
\begin{aligned}
V_1 &= AP \sum_{n=1,3,5,\ldots}^{N} \frac{h_0^{(n)}}{n!} \left(\frac{R^n}{2^{n-1}}\right) \frac{n!}{(\frac{n-1}{2})!(\frac{n+1}{2})!} \\
&= 2AP \sum_{m=0}^{M_1} \frac{h_0^{(2m+1)}}{m!(m+1)!} \left(\frac{R}{2}\right)^{2m+1}
\end{aligned}
\tag{S30}
$$

where $M_1 = \text{floor}((N-1)/2)$. Lastly, V_2 is found by substituting $n - 2k = 2$ into Eq. S27 and Eq. S26. Only even $n \geq 2$ contribute to this sum:

$$V_2 = AP \sum_{n=2,4,6,\dots}^{N} \frac{h_0^{(n)}}{n!} \left(\frac{R^n}{2^{n-1}} \right) \frac{n!}{(\frac{n}{2}-1)!(\frac{n}{2}+1)!}$$

$$= 2AP \sum_{m=0}^{M_2} \frac{h_0^{(2m+2)}}{m!(m+2)!} \left(\frac{R}{2} \right)^{2m+2} \tag{S31}$$

where $M_2 = \text{floor}((N-2)/2)$. Interestingly, if we take $N \to \infty$ these sums bear remarkable resemblance to modified Bessel functions of the first kind:

$$I_\alpha(x) = \sum_{m=0}^{\infty} \frac{1}{m!(m+\alpha)!} \left(\frac{x}{2} \right)^{2m+\alpha} \tag{S32}$$

Thus for the case of $N \to \infty$ we may write $V_0 \dots V_2$ as:

$$V_0 = -\frac{1}{\tau} T_0 + API_0 \left(R\frac{d}{dx} \right) \cdot h(x) \Big|_{x=0} \tag{S33}$$

$$V_1 = 2API_1 \left(R\frac{d}{dx} \right) \cdot h(x) \Big|_{x=0} \tag{S34}$$

$$V_2 = 2API_2 \left(R\frac{d}{dx} \right) \cdot h(x) \Big|_{x=0} \tag{S35}$$

In fact, it can be shown that for all $n > 0$ the temperature variation at frequency $n\omega$ is given by:

$$V_n = 2API_n \left(R\frac{d}{dx} \right) \cdot h(x) \Big|_{x=0} \tag{S36}$$

Of course, in the $N \to \infty$ limit we also have $h(x) = g(x + z_0)$.

If we truncate $h(x)$ at $N = 7$, then we have $M_0 = 3$ in Eq. S29. Therefore by Eq. S18, the time-averaged change in temperature is given by:

$$\tau V_0 = -T_0 + \tau AP \sum_{m=0}^{3} \frac{h_0^{(2m)}}{(m!)^2} \left(\frac{R}{2} \right)^{2m} \tag{S37}$$

Furthermore, when $N = 7$ we have $M_1 = 3$ and $M_2 = 2$ in Eqs. S30 & S31. Thus V_1 contains all odd powers of R from R^1 to R^7, and V_2 contains all even powers from R^2 to R^6. Upon substituting V_1 and V_2 into Eq. S22, we then finally arrive at our equation for R:

$$0 = c_0 + c_1 R^2 + c_2 R^4 + c_3 R^6 \tag{S38}$$

where

$$c_0 = \frac{\omega_1^2 D}{1 + \omega_1^2 \tau^2} h_0^{(1)} + \frac{1}{\tau^2 APQ}$$

$$c_1 = \frac{\omega_1^2 D}{1 + \omega_1^2 \tau^2} \frac{h_0^{(3)}}{2^2 1! 2!} - \frac{C}{1 + 4\omega_1^2 \tau^2} \frac{h_0^{(2)}}{2^1 0! 2!}$$

$$c_2 = \frac{\omega_1^2 D}{1 + \omega_1^2 \tau^2} \frac{h_0^{(5)}}{2^4 2! 3!} - \frac{C}{1 + 4\omega_1^2 \tau^2} \frac{h_0^{(4)}}{2^3 1! 3!}$$

$$c_3 = \frac{\omega_1^2 D}{1 + \omega_1^2 \tau^2} \frac{h_0^{(7)}}{2^6 3! 4!} - \frac{C}{1 + 4\omega_1^2 \tau^2} \frac{h_0^{(6)}}{2^5 2! 4!}$$

The results shown above are expressed in dimensionless units. When re-dimensionalized, they reproduce Eq. 5 of the main text. The ϵ^1-order correction to the resonant frequency is (upon rearranging Eq. S23)

$$\omega_2 = \frac{\tau C}{2\omega_1} V_0 - \frac{\omega_1 \tau D}{1 + \omega_1^2 \tau^2} \frac{V_1}{2R} + \frac{\tau C}{1 + 4\omega_1^2 \tau^2} \frac{V_2}{4\omega_1} \tag{S39}$$

When $h(x)$ is truncated at $N = 7$ this becomes

$$\omega_2 = d_0 + d_1 R^2 + d_2 R^4 + d_3 R^6 \tag{S40}$$

where (again in dimensionless units)

$$d_0 = -\frac{\omega_1 \tau D}{1 + \omega_1^2 \tau^2} \frac{A P h_0^{(1)}}{2^1 0! 1!} + \frac{\tau C}{2\omega_1} \left(-\frac{1}{\tau} T_0 + A P h_0^{(0)} \right)$$

$$d_1 = -\frac{\omega_1 \tau D}{1 + \omega_1^2 \tau^2} \frac{A P h_0^{(3)}}{2^3 1! 2!} + \frac{\tau C}{1 + 4\omega_1^2 \tau^2} \frac{A P h_0^{(2)}}{2^3 0! 2! \omega_1}$$

$$d_2 = -\frac{\omega_1 \tau D}{1 + \omega_1^2 \tau^2} \frac{A P h_0^{(5)}}{2^5 2! 3!} + \frac{\tau C}{1 + 4\omega_1^2 \tau^2} \frac{A P h_0^{(4)}}{2^5 1! 3! \omega_1}$$

$$d_3 = -\frac{\omega_1 \tau D}{1 + \omega_1^2 \tau^2} \frac{A P h_0^{(7)}}{2^7 3! 4!} + \frac{\tau C}{1 + 4\omega_1^2 \tau^2} \frac{A P h_0^{(6)}}{2^7 2! 4! \omega_1}$$

S2.   STATIC NANOWIRE BEHAVIOR

From Eqs. S1 & S2 the static nanowire must satisfy

$$z_0 = DT_0 \tag{S41}$$

$$\frac{1}{\tau}T_0 = APg(z_0) \tag{S42}$$

Rearranging these shows that the nanowire equilibrium is determined by the roots of the following equation:

$$0 = APg(z_0) - \frac{z_0}{\tau D} \tag{S43}$$

Near $P = 0$ this equation has only one root, but as P increases more roots develop. This function is plotted for multiple P values in Fig. S1 (a) for $\phi = 0$. The upper panel displays the lowest valid solution of Eq. S43, which has a discontinuous jump in z_0 from one crest of $g(z)$ to the next as P increases quasi-statically. These results suggest that for high enough P values, z_0 will reside only in regions of $g(z)$ with negative slope dg/dz – i.e. in regions conducive to self-oscillation. It should be noted that in this experiment (and in the function plotted in Fig. S1), a positive D value is assumed. If we were to invert our spatial coordinates, we would have $D < 0$, and the equilibrium z_0 would shift towards negative values for increasing P; the tendency of z_0 to reside only in regions conducive to self-oscillation (regions of positive dg/dz in this case) would still be observed.

Fig. S1 (b-d) show the expected equilibrium position for our nanowire based on Eq. S43 for varying ϕ and P values. Fig. S1 (b) displays the equilibrium shift relative to the $P = 0$ position (i.e. z_0), which is periodic in $\lambda/2$ as expected. Fig. S1 (c) displays the absolute nanowire position within the standing wave (i.e. $z_0 + \phi$), and the slope dg/dz at this absolute position is shown in Fig. S1 (d).

Labeling Eq. S43 by $f(z_0) = APg(z_0) - \frac{z_0}{\tau D}$, we prove in Section S4 that equilibrium points (z_0, T_0) at which the the local slope $df/dz_0 > 0$ are unstable. Therefore when P is large enough such that $f(z_0)$ has multiple roots, only those
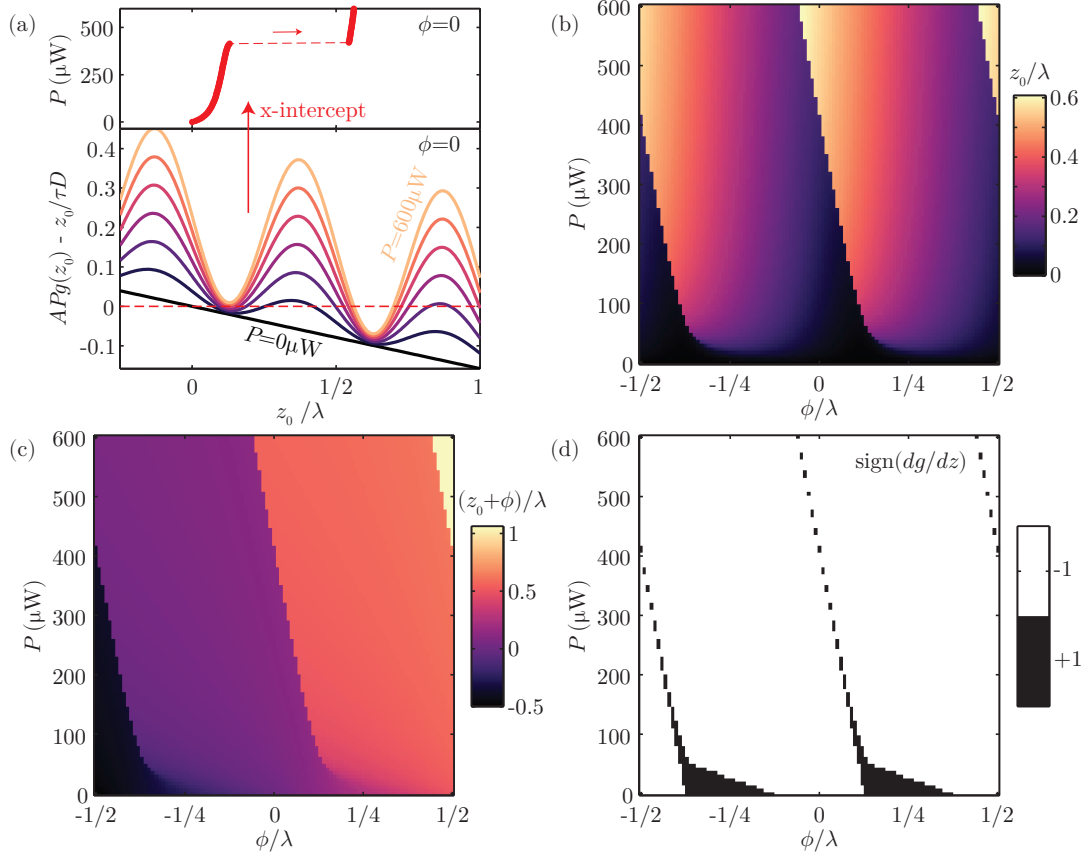

FIG. S1. Equilibrium position of the static nanowire vs laser power P and initial position ϕ

roots with negative local slope $df/dz_0 < 0$ represent viable equilibrium points (z_0, T_0). This further suggests that at high enough laser powers only equilibrium points conducive to self-oscillation (i.e. with $dg/dz < 0$) are allowed.

S3.   CRITICAL POWER AND HYSTERESIS

Reproducing a result from Section S1, the amplitude R of self-oscillation is (in dimensionful units):

$$0 = c_0 + c_1 R^2 + c_2 R^4 + c_3 R^6 \tag{S44}$$

where

$$c_0 = \frac{\omega_1^2 D}{1 + \omega_1^2 \tau^2} \, g_{z_0}^{(1)} + \frac{\gamma}{\tau^2 AP}$$

$$c_1 = \frac{\omega_1^2 D}{1 + \omega_1^2 \tau^2} \frac{g_{z_0}^{(3)}}{2^2 1! 2!} - \frac{\omega_{0i}^2 C}{1 + 4\omega_1^2 \tau^2} \frac{g_{z_0}^{(2)}}{2^1 0! 2!}$$

$$c_2 = \frac{\omega_1^2 D}{1 + \omega_1^2 \tau^2} \frac{g_{z_0}^{(5)}}{2^4 2! 3!} - \frac{\omega_{0i}^2 C}{1 + 4\omega_1^2 \tau^2} \frac{g_{z_0}^{(4)}}{2^3 1! 3!}$$

$$c_3 = \frac{\omega_1^2 D}{1 + \omega_1^2 \tau^2} \frac{g_{z_0}^{(7)}}{2^6 3! 4!} - \frac{\omega_{0i}^2 C}{1 + 4\omega_1^2 \tau^2} \frac{g_{z_0}^{(6)}}{2^5 2! 4!}$$

Here we have made the approximation $h(x) = g(x + z_0)$. This can be rearranged to express P as a function of R:

$$P = \frac{-\gamma/(\tau^2 A)}{b + c_1 R^2 + c_2 R^4 + c_3 R^6} \tag{S45}$$

where $b = (\omega_1^2 D g_{z_0}^{(1)})/(1 + \omega_1^2 \tau^2)$. The critical laser power P_{crit} is simply the $R = 0$ value of this function:

$$P_{\text{crit}} = -\frac{\gamma \left(1 + \omega_1^2 \tau^2\right)}{\omega_1^2 \tau^2 D A g_{z_0}^{(1)}} \tag{S46}$$

Whether the transition to self-oscillation will be hysteretic or non-hysteretic (i.e. whether the Hopf bifurcation will be subcritical or supercritical) is determined by the curvature $d^2 P/dR^2$ at $R = 0$. Upon differentiating Eq. S45 twice, one finds that this curvature is given by

$$\left.\frac{d^2 P}{dR^2}\right|_{R=0} = \frac{2\gamma c_1}{\tau^2 A b^2} \tag{S47}$$

Because physical values of γ and A must be positive, this result suggests that $c_1 < 0$ is the necessary condition for a hysteretic transition. Such a transition is depicted in Fig. S2. The parameters used to produce this figure are identical to the experimental values of our nanowire, except C has been increased by a factor of 100; ϕ is near $\lambda/8$, where $|g_{z_0}^{(2)}|$
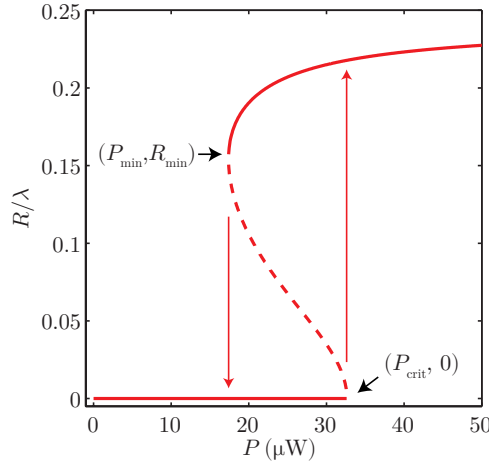

FIG. S2. A subcritical Hopf bifurcation. A dashed line indicates unstable behavior.

is maximal. In this figure z_0 (the time-averaged position) has been held fixed over the entire P range to simplify the results.

The width of the hysteresis region can be found by analyzing the first derivative of P:

$$\frac{dP}{dR} = \frac{\gamma}{\tau^2 A} \frac{2c_1 R + 4c_2 R^3 + 6c_3 R^5}{(b + c_1 R^2 + c_2 R^4 + c_3 R^6)^2} \tag{S48}$$

As seen in Fig. S2, the minimum P value at which self-oscillation is sustainable coincides with a turning point in $P(R)$ – i.e. it occurs when $dP/dR = 0$. Note that $dP/dR = 0$ also occurs at $R = 0$ – i.e. at the critical power $P = P_{\text{crit}}$. The lower edge of the self-oscillation region is thus found by solving the following equation for the minimum amplitude R_{min}

$$0 = 2c_1 + 4c_2 R^2 + 6c_3 R^4 \tag{S49}$$

and substituting the resulting value back into Eq. S45 for P to give $P_{\text{min}} = P(R_{\text{min}})$. This calculation seems straightforward if c_1, c_2, and c_3 are taken as constants, but in actuality these quantities are dependent on z_0, which generally depends on P; this makes calculation of P_{min} much more difficult. Therefore one approach to calculating P_{min} would be to iteratively solve Eqs. S49, S45 & S43 for R, P, and z_0 until they converge on fixed values.

S4.   NOTE ABOUT LYAPUNOV STABILITY

In Section S1, we found a solution for the position and temperature of our resonator by assuming a displacement of the form $x(t) = R\cos\omega t$ and applying perturbation theory to Eqs. S3 & S4. In the end, we determined the oscillation amplitude R as a function of laser power P (Eq. S38). We also determined the critical power P_{crit} required for self-oscillation (Eq. S46). However, knowing that one effect of the Cu term in Eq. S3 is to modulate the resonant frequency of the system at a rate of 2ω, or twice the oscillation frequency (as demonstrated by the V_2 term in Eq. S22), we might reasonably wonder whether this parametric modulation by C can in its own right produce self-oscillation. After all, setting $D = 0$ leads to $P_{\text{crit}} \to \infty$ (suggesting that the system will never self-oscillate), but also leads Eq. S3 to resemble the damped Mathieu equation, given by

$$\ddot{x} + \gamma\dot{x} + \omega_0^2\left(1 + \delta\cos 2\omega_0 t\right)x = 0 \tag{S50}$$

in which the equilibrium state $x = \dot{x} = 0$ is known to become unstable once the modulation strength δ is large enough[1] ($\delta > \frac{2\gamma}{\omega_0}$). Despite this resemblance, our system in fact will not oscillate if $D = 0$, and only laser powers $P > P_{\text{crit}}$ (with P_{crit} given by Eq. S46) will result in self-oscillation. Moreover, if $P > P_{\text{crit}}$ the system has no choice but to oscillate. In this section, we will prove these assertions by examining the Lyapunov stability of Eqs. S3 & S4 at the equilibrium point $x = \dot{x} = u = 0$.

Restating Eqs. S3 & S4 with $h(x) = g(x + z_0)$:

$$\ddot{x} + \gamma\dot{x} + \omega_{0i}^2(1 + CT_0 + Cu)(x - Du) = 0 \tag{S51}$$

$$\dot{u} + \frac{1}{\tau}u = -\frac{1}{\tau}T_0 + APh(x) \tag{S52}$$

$$= AP\left[h_0^{(1)}x + \frac{1}{2!}h_0^{(2)}x^2 + \frac{1}{3!}h_0^{(3)}x^3 + \dots\right]$$

In the second of these equations we have expanded $h(x)$ in a Taylor series and made use of the fact that $APh(0) = \frac{T_0}{\tau}$. Defining $\omega_1^2 = \omega_{0i}^2(1 + CT_0)$, we can rewrite this as a system of first order differential equations:

$$\dot{x} = y \tag{S53}$$

$$\dot{y} = -\omega_1^2 x - \gamma y + \omega_1^2 Du - \omega_{0i}^2 Cux + \omega_{0i}^2 CDu^2 \tag{S54}$$

$$\dot{u} = -\frac{1}{\tau}u + AP\left[h_0^{(1)}x + \frac{1}{2!}h_0^{(2)}x^2 + \frac{1}{3!}h_0^{(3)}x^3 + \dots\right] \tag{S55}$$

or, in matrix form:

$$\frac{d}{dt}\begin{bmatrix} x \\ y \\ u \end{bmatrix} = \begin{bmatrix} 0 & 1 & 0 \\ -\omega_1^2 & -\gamma & \omega_1^2 D \\ APh_0^{(1)} & 0 & -\frac{1}{\tau} \end{bmatrix}\begin{bmatrix} x \\ y \\ u \end{bmatrix} + G\begin{bmatrix} x \\ y \\ u \end{bmatrix} \tag{S56}$$

G above is a matrix of strictly nonlinear (i.e. quadratic and higher order) terms. Referring to the preceding matrix of linear terms as F, we know that $x = y = u = 0$ is asymptotically Lyapunov stable if all the eigenvalues of F have negative real parts, and it is Lyapunov unstable if at least one eigenvalue has a positive real part.[1,2] In these cases, no matter what nonlinear terms are contained in G, they will not affect the stability of the system. Only if the eigenvalues of F are purely imaginary would the nonlinear terms determine the stability. So we now proceed to determine the eigenvalues of F. This leads to:

$$\begin{vmatrix} -\lambda & 1 & 0 \\ -\omega_1^2 & -\gamma - \lambda & \omega_1^2 D \\ APh_0^{(1)} & 0 & -\frac{1}{\tau} - \lambda \end{vmatrix} = 0 \tag{S57}$$

which gives us

$$\lambda^3 + a\lambda^2 + b\lambda + c = 0 \tag{S58}$$

where

$$a = \gamma + \frac{1}{\tau} \tag{S59}$$

$$b = \frac{\gamma}{\tau} + \omega_1^2 \tag{S60}$$

$$c = \omega_1^2\left(\frac{1}{\tau} - APh_0^{(1)}D\right) \tag{S61}$$

11

Note that $a, b > 0$ because the physical quantities γ, τ, ω_1 are all positive. The sign of c, however, depends on the product $APh_0^{(1)}D$. If we now break λ into real and imaginary components $\lambda = \eta + i\theta$, we can similarly separate Eq. S58:

$$\text{Real part of Eq. S58:} \quad \eta^3 - 3\eta\theta^2 + a(\eta^2 - \theta^2) + b\eta + c = 0 \tag{S62}$$

$$\text{Imaginary part of Eq. S58:} \quad 3\eta^2\theta - \theta^3 + 2a\eta\theta + b\theta = 0 \tag{S63}$$

Solving Eq. S63 for θ gives:

$$\theta = 0 \tag{S64}$$

$$\theta = \pm\sqrt{3\eta^2 + 2a\eta + b} \tag{S65}$$

Upon substitution into Eq. S62, these lead to:

$$\eta^3 + a\eta^2 + b\eta + c = 0 \tag{S66}$$

$$8\eta^3 + 8a\eta^2 + 2(a^2 + b)\eta + ab - c = 0 \tag{S67}$$

Because $a, b > 0$, the first of these can only result in $\eta > 0$ if $c < 0$. Similarly, the second equation above will only lead to $\eta > 0$ if $ab - c < 0$. Substituting in the definitions of a, b, c, the equilibrium point $x = y = u = 0$ is therefore Lyapunov unstable if either of the following is satisfied:

$$APh_0^{(1)}D - \frac{1}{\tau} > 0 \tag{S68}$$

$$\left(\gamma + \frac{1}{\tau}\right)\left(\frac{\gamma}{\tau} + \omega_1^2\right) - \omega_1^2\left(\frac{1}{\tau} - APh_0^{(1)}D\right) < 0 \tag{S69}$$

or, upon rearranging:

$$APh_0^{(1)}D > \frac{1}{\tau} \tag{S70}$$

$$-APh_0^{(1)}D > \frac{\gamma(1 + \omega_1^2\tau^2) + \gamma^2\tau}{\omega_1^2\tau^2} \tag{S71}$$

We recognize Eq. S70 as being closely related to Eq. S43, which defines the equilibrium point (z_0, T_0). In fact, Eq. S70 represents the first derivative of Eq. S43 with respect to z_0 (bearing in mind that $h_0^{(1)} = g_{z_0}^{(1)}$). This proves that any equilibrium point (z_0, T_0) satisfying Eq. S70 is unstable. Note that this only affects equilibrium points (z_0, T_0) with $h_0^{(1)} > 0$ – i.e. regions of $g(z)$ that do not support self-oscillation. Furthermore, because the eigenvalue is purely real ($\theta = 0$) in this case, this instability is not accompanied by oscillations in $x, \dot{x}, u$.

In contrast to Eq. S70, Eq. S71 can only hold if $h_0^{(1)} < 0$. In fact, this is a reproduction of the critical power P_{crit} defined by Eq. S46 (and Eq. 6 of the main text) with one small addition: the $\gamma^2\tau$ term. This term is missing from our previous derivations of P_{crit} because in applying perturbation theory, we scaled γ by a small parameter ϵ (see Eq. S14) and neglected terms of order ϵ^2 and higher. This then proves our previous assertions that for $P < P_{\text{crit}}$ our system will not oscillate, and for $P > P_{\text{crit}}$ it has no choice but to oscillate.

S5. DEVICE FABRICATION

One of the goals during fabrication of these nanowire devices was to create a MEMS/NEMS structure which would be useful over a wide range of temperatures. Stoichiometric Silicon Nitride (Si_3N_4) was chosen as the nanowire material for its high stress and high quality factors.[3] The Niobium coating was specified so that the superconducting material can (in the future) be coupled to a SQUID (Superconducting QUantum Interference Device) detector for ultralow temperature use.[4,5] In such a configuration, feedback from the SQUID can be used to induce self-oscillation in a manner equivalent to the photothermal feedback studied here at room temperature. A major advantage of these devices for low-temperature studies is that the nanowire cross-sections ($\approx 50\,nm$) are smaller than the superfluid ^{3}He pair size ($70\,nm$ at low pressure). The nanowires would thus be minimally invasive to the superfluid and enable new studies of fundamental physics in this system.[6]

The nanowires and supporting cantilevers were patterned using a combination of electron-beam lithography and optical lithography. Misalignment between these steps caused a slight difference in the cantilever lengths for a given device (discussed in the next section). Combining these two lithography technologies allowed for definition of very small features (the $50\,nm$-wide nanowires), but also allowed for definition of the larger features (the surrounding trenches) in a short exposure time.

The process flow was as follows: Deposit $25\,nm$ of Si_3N_4 on a Silicon wafer by Low Pressure Chemical Vapor Deposition (LPCVD). Then, deposit $50\,nm$ of Titanum/Gold and pattern via optical lithography and lift-off to define contact pads on either end of the nanowire trench; these contact pads were not used in this work, but will be used to make electrical contact to a SQUID detector in low-temperature experiments. Then, define the nanowires and supporting paddles in resist using electron-beam lithography, followed by defining of the trench boundaries using optical lithography. This is followed by etching of the Si_3N_4 using a CHF_3/O_2 plasma etch. The underlying Si was then etched to a depth of $8\,\mu m$ using a wet KOH etch. The sample was then dried using a CO_2 critical point dryer, followed by deposition of the $20\,nm$ Nb film. A scanning electron micrograph of two neighboring nanowires is shown in Figure S3.

We note that although there is a thin coating of Nb on the trench floor as well as on the nanowire from sputter deposition, the choice was made to model this surface optically as being pure Si. The reflectivities of bulk Si and Nb in the visible range are roughly 35% and 55%, respectively, and the reflectivity of this composite surface is between these values. For simplicity we have chosen to use the pure Si value to compute α and β in our model (see Eq. S3 and Eqs. S82 & S83); this assumption may affect the measured value of A in our experiment slightly, but does not affect the overall model any more than the uncertainty in α and β arising from the Gaussian nature of our laser beam, as discussed in Section S8.
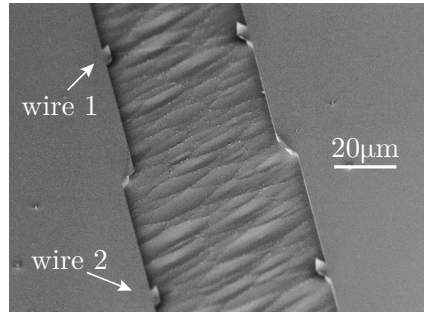

FIG. S3. Angled scanning electron microscopy image of two neighboring nanowires, one of $40\,\mu m$ length (top) and another of $50\,\mu m$ length (bottom).

S6.   ESTIMATION OF THERMAL PARAMETERS

The mechanical and thermal parameters of our system (ω_0, τ, C, D) can be accurately estimated by knowledge of the material composition of our nanowire and the cantilevers by which it is suspended. The optical parameters (A, α, β) require also knowledge of our laser spot size and the refractive index of the reflective silicon back-plane.

The resonant frequency of a tensioned wire composed of a single material with Young's modulus E and internal strain ε is

$$\omega_0 = \frac{\pi}{L}\sqrt{\frac{E\varepsilon}{\rho}} \tag{S72}$$

where L is the wire length and ρ is the mass per unit volume. This equation neglects terms due to bending of the wire, and is valid only in the high tension limit. For a wire composed of two distinct materials, this becomes

$$\omega_0 = \frac{\pi}{L}\sqrt{\frac{\sigma_{\text{tot}}}{\mu_{\text{tot}}}} = \frac{\pi}{L}\sqrt{\frac{E_1 A_1 \varepsilon_1 + E_2 A_2 \varepsilon_2}{\rho_1 A_1 + \rho_2 A_2}} \tag{S73}$$

where $\sigma_{\text{tot}}, \mu_{\text{tot}}$ are the total tensile stress and mass per unit length of the wire. The subscripts $1, 2$ have been used to distinguish between the two materials and A_n is the cross-sectional area of either material.

The parameter C, which denotes the fractional stress change per unit temperature in Eq. S1 can be approximated by

$$C = \frac{1}{\sigma_{\text{tot}}}\left(\frac{d\sigma_{\text{tot}}}{dT}\right) \approx -\frac{E_1 A_1 \alpha_1 + E_2 A_2 \alpha_2}{E_1 A_1 \varepsilon_1 + E_2 A_2 \varepsilon_2} \tag{S74}$$

Here α_n is the linear thermal expansion coefficient of material n, and this effect is entirely attributed to tension change within the wire. We have assumed here that as the temperature changes both materials are free to expand and do not influence one another. This is not entirely accurate because the two materials are coupled at their interface. A more accurate calculation would incorporate the effective thermal expansion coefficient α_{eff} of the joined materials, which would have a value between $\alpha_1 \approx 3 \times 10^{-6} \text{K}^{-1}$ and $\alpha_2 \approx 7 \times 10^{-6} \text{K}^{-1}$. Hence this would not produce a substantially different value for C.

The parameter D describes coupling between temperature and the vertical position of our nanowire. This coupling is caused by the bimetalic cantilevers on either end of the nanowire, which at room temperature ($\approx 300\,\text{K}$) curve upward due to unbalanced stresses between the Nb film (top layer) and the underlying SiN. A detailed calculation of D based on cantilever dimensions is presented in Section S7. Here we estimate D for a single nanowire based on angled-SEM (Scanning Electron Microscopy) measurements of the cantilever length l_c and equilibrium angle θ above the horizontal. If θ is known, an estimate for D can be obtained by modeling the cantilever as acting under the influence of an internal torque $\mathcal{T}_c$ which pulls it up and nanowire tension σ_{tot} which pulls it along the horizontal. Relative to a rotation axis at the cantilever clamped edge, the torque exerted by the nanowire is $\sigma_{\text{tot}} l_c \sin\theta$; in equilibrium we must therefore have $\mathcal{T}_c = \sigma_{\text{tot}} l_c \sin\theta$. The vertical position of the cantilever free end is $z = l_c \sin\theta$. If the two cantilevers supporting the nanowire have differing lengths l_{c1}, l_{c2} and equilibrium angles θ_{c1}, θ_{c2}, then the vertical position of the nanowire center is:

$$z = \frac{l_{c1} \sin\theta_{c1} + l_{c2}\sin\theta_{c2}}{2} = \frac{\mathcal{T}_{c1} + \mathcal{T}_{c2}}{2\sigma_{\text{tot}}} \tag{S75}$$

The change in vertical position of the nanowire per unit temperature change is then

$$D \approx -\left(\frac{\mathcal{T}_{c1} + \mathcal{T}_{c2}}{2\sigma_{\text{tot}}^2}\right)\left(\frac{d\sigma_{\text{tot}}}{dT}\right) \approx \left(\frac{\mathcal{T}_{c1} + \mathcal{T}_{c2}}{2}\right)\frac{E_1 A_1 \alpha_1 + E_2 A_2 \alpha_2}{\left(E_1 A_1 \varepsilon_1 + E_2 A_2 \varepsilon_2\right)^2} \tag{S76}$$

This formula holds only for small deviations away from the equilibrium angles θ_{c1}, θ_{c2}. As with C, this parameter is proportional to the change in wire stress per unit temperature.

For a heated mechanical resonator composed of a single material, the thermal time constant τ would simply be:

$$\tau = \frac{L_{\text{eff}}}{\Lambda A_{\text{eff}}}\,\rho c V_{\text{eff}} \tag{S77}$$

where Λ, c are the thermal conductivity and specific heat of the material, and $L_{\text{eff}}, A_{\text{eff}}$ are the effective length and cross section of the conductive channel. V_{eff} is the effective volume of heated material, and the combination $\rho c V_{\text{eff}}$ is the thermal mass. The combination $L_{\text{eff}}/(\Lambda A_{\text{eff}})$ is the thermal resistance.

In our system, heat flows from the nanowire midpoint (where the laser is focused) out to the clamped edges of the two cantilevers. It flows in parallel paths through the SiN (material 1) and Nb (material 2), along two possible directions out from the midpoint. The thermal resistance of the nanowire (from midpoint to endpoint) is $R_w = (1/2)L/(\Lambda_1 A_1 + \Lambda_2 A_2)$. The resistance of either cantilever is $R_c = l_c/(\Lambda_1 A_{c1} + \Lambda_2 A_{c2})$. Because of the two directions outward from the midpoint, the total resistance is $R_{\text{tot}} = (R_w + R_c)/2$. The total thermal mass μ of the system (assuming cantilevers of equal length l) is given by $\mu_{\text{tot}} = c_1 \rho_1 (LA_1 + 2l_c A_{c1}) + c_2 \rho_2 (LA_2 + 2l_c A_{c2})$. Therefore the thermal time is

$$\tau = \mu_{\text{tot}} R_{\text{tot}} \tag{S78}$$

The A parameter in Eq. S2 can be expressed as:

$$A = \frac{a}{\mu_{\text{tot}}} = \frac{[1 - \exp\left(-4\pi k_{Nb} t_{Nb}/\lambda\right)] \operatorname{erf}\left(\sqrt{2}\, w/d_L\right)}{\mu_{\text{tot}}} \tag{S79}$$

Here, a denotes the fraction of local laser light absorbed by the nanowire; k_{Nb}, t_{Nb} are the extinction coefficient and thickness of the Nb film, and w is the width of the nanowire. The diameter of our Gaussian laser beam is denoted by d_L, and the error function $\operatorname{erf}(\sqrt{2}w/d_L)$ represents the fraction of laser beam cross-sectional area that is covered by the thin nanowire (assuming it lies along the center of the laser beam). The terms in square brackets denote the fraction of light within that thin area that is absorbed by the Nb film.

The nanowire sits in an optical standing wave generated by interference between incident light from our laser and light reflected from the silicon backplane. If we approximate the light as plane waves, it can be shown that in the presence of such a reflector the optical intensity varies with distance as

$$P(z) = P_0(1 + R_0) - 2P_0\sqrt{R_0} \sin\left(\frac{4\pi z}{\lambda}\right) \tag{S80}$$

where P_0 corresponds to the incident laser power and R_0 is the reflection coefficient. Note that $P(z)$ here denotes the total energy density $P(z) = |\vec{E}(z)|^2$ of the light in plane z, where $\vec{E}$ is the combined electric field of the incident and reflected beams. Similarly, $P_0 = |\vec{E}_0|^2$ for the incident beam. Note also that in Eq. S3 and Eq. 3 of the main text, a shift of ϕ is introduced to account for the resonator's arbitrary initial ($z = 0$) position relative to the mirror.

This is related to the index of refraction of the silicon, $n_{Si} = 3.87 + 0.01i$ at 640 nm (Ref. 7), by

$$R_0 = \left|\frac{n_{\text{Si}} - 1}{n_{\text{Si}} + 1}\right|^2 \approx 0.35 \tag{S81}$$

Thus the two remaining parameters in Eq. S2 are given by

$$\alpha = 1 + R_0 \tag{S82}$$
$$\beta = 2\sqrt{R_0} \tag{S83}$$

Because the nanowire is much thinner than both the wavelength λ and spot size R_L, we have assumed that it does not greatly affect the optical standing wave in Eq. S80.

Table S1 lists the relevant material properties for SiN and Nb. Tables S2 & S3 list the resulting mechanical and thermal parameters of our system. In Table S2, all values have been measured experimentally except for those marked with asterisks (*), which were calculated based on Eq. S73. In Table S3, A excludes the error function shown in Eq. S79 since d_L (the laser spot diameter) was used as a fit parameter during the experiment. The other fit parameters were $1/\tau$ (the cooling rate) and ϕ, the initial position of the nanowire within the optical field, as seen in Eq. S3. Typical d_L values arising from the fits were 2μm to 2.5μm.

	SiN	Nb	Units	Description	References
ρ	3000	8600	$\mathrm{kg\,m^{-3}}$	mass density	8 & 9
Y	290	105	GPa	Young's modulus	8 & 9
α	3	7	$10^{-6}\,\mathrm{K^{-1}}$	thermal expansion coeff.	10 & 9
Λ	22	54	$\mathrm{Wm^{-1}K^{-1}}$	thermal conductivity	8 & 9
c	700	265	$\mathrm{Jkg^{-1}K^{-1}}$	specific heat	8 & 9
k	0	3.36		extinction coefficient	11

TABLE S1. Material parameters used for SiN & Nb

	Value	Units	Description
$\omega_0/2\pi$	3.03	MHz	resonant frequency
A_1	875	$\mathrm{nm^2}$	wire SiN cross-section
A_2	1420	$\mathrm{nm^2}$	wire Nb cross-section
$\varepsilon_{\mathrm{SiN}}$	0.3	%	*strain
$\varepsilon_{\mathrm{Nb}}$	0.02	%	*strain
t_{Nb}	20	nm	Nb thickness
w	51	nm	wire width
L	40	μm	wire length
l_{c1}	2.4	μm	cantilever length
l_{c2}	4.1	μm	cantilever length
θ_1	16°		cantilever angle
θ_2	11°		cantilever angle
A_{c1}	1.41	$10^{-13}\,\mathrm{m^2}$	cantilever SiN cross-section
A_{c2}	1.13	$10^{-13}\,\mathrm{m^2}$	cantilever Nb cross-section

TABLE S2. Mechanical parameters of our nanowire

	Theoretical Value	Value From Fit	Units
A	1.87	–	$10^{11}\,\mathrm{K\,J^{-1}}$
$1/\tau$	2.49	7.46	kHz
C	-2.21	–	$10^{-3}\,\mathrm{K^{-1}}$
D	1.64	–	$\mathrm{nm\,K^{-1}}$
α	0.171	–	
β	2.344	–	

TABLE S3. Photo-thermal parameters of our nanowire

S7.   BEAM THEORY FOR SUPPORTING CANTILEVERS

The supporting cantilevers at either end of our nanowire are composed of a layer of stressed SiN coated with a thin film (20 nm) of Nb. The Nb was deposited by sputter deposition. In this section we assume that the unbalanced stresses which cause the cantilevers to curl upward are entirely thermally induced – i.e. arising due to differing thermal expansion coefficients in the two layers and deposition of Nb atoms at a temperature $\gg 300\,\mathrm{K}$. Internal stresses in the sputtered film can also contribute to the overall stress, but will not affect the scaling of our coupling constant D with cantilever dimensions.

We begin by calculating the neutral axis of a two-material composite beam. It is located a distance $\bar{y}$ above the bottom surface of the lower material (material 2). During bending, the stresses above and below the neutral axis must balance to zero. For two homogeneous materials (moduli E_1, E_2) of equal width and uniform thicknesses h_1, h_2, this condition simplifies to $0 = E_1 h_1 y_1 + E_2 h_2 y_2$. Here $y_1 = h_2 + h_1/2 - \bar{y}$ and $y_2 = h_2/2 - \bar{y}$ are the distances from the centers of materials 1 and 2 to the neutral axis. The neutral axis is therefore located at:

$$\bar{y} = \frac{\left(h_2 + \frac{h_1}{2}\right)\frac{E_1}{E_2}h_1 + \frac{1}{2}h_2^2}{\frac{E_1}{E_2}h_1 + h_2} \tag{S84}$$

This is depicted in Fig. S4. A simplification we can make in analyzing the composite beam is to use an equivalent area to represent the increased stiffness of material 1 (the Nb). This is also depicted in Fig. S4. Both materials are now assumed to have modulus E_2, but the top material has an effective width bE_1/E_2 compared to the original b. The area moment of inertia of the beam relative to this axis is:

$$I = \bar{I}_1 + \bar{A}_1 y_1^2 + \bar{I}_2 + \bar{A}_2 y_2^2 \tag{S85}$$

where

$$\bar{I}_1 = \frac{E_1}{E_2}\frac{bh_1^3}{12} \qquad \bar{I}_2 = \frac{bh_2^3}{12}$$
$$\bar{A}_1 = \frac{E_1}{E_2}bh_1 \qquad \bar{A}_2 = bh_2$$

Above $\bar{I}_1, \bar{I}_2$ are the moments of inertial relative to the center axes of the two materials, and the parallel axis theorem has been applied. Because we have used E_2 as the reference modulus, the bending stiffness of the composite beam is

$$K = E_2 I. \tag{S86}$$

In the absence of tensile force from the nanowire, either cantilever should have constant curvature κ due to its internal/thermal stresses. Approximating this curvature by $\kappa = d^2 z/dx^2$, where $z(x)$ is the vertical position of the cantilever a distance x from its clamping point, leads to a deflection profile of $z(x) = (1/2)\kappa x^2$. Therefore the height of the cantilever end is $z_{\max} = (1/2)\kappa l_c^2$, where l_c is the cantilever length. If the curvature is entirely thermally-induced, it is given by:[12]

$$\kappa = \frac{6E_1 E_2 (h_1 + h_2) h_1 h_2 (\alpha_1 - \alpha_2)\Delta T}{E_1^2 h_1^4 + 4E_1 E_2 h_1^3 h_2 + 6E_1 E_2 h_1^2 h_2^2 + 4E_1 E_2 h_1 h_2^3 + E_2^2 h_2^4} \tag{S87}$$
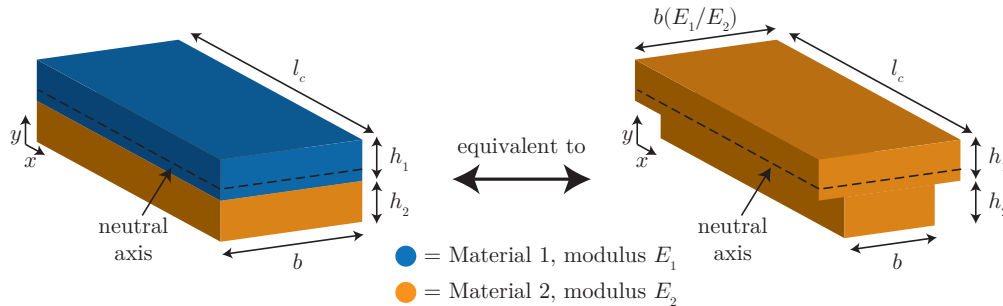

FIG. S4. Equivalent views of the composite cantilever according to beam theory
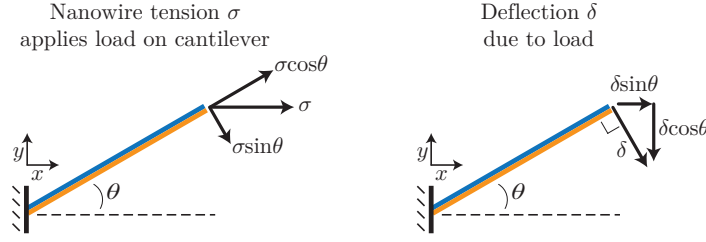
FIG. S5. Behavior of the composite beam under load

where α_1, α_2 are the thermal expansion coefficients of the two materials and ΔT is the temperature change relative to a reference temperature (the Nb deposition temperature). Other internal stresses in the two materials may contribute to κ, however, so the remaining equations will be presented for a general κ.

Shown in Fig. S5 is the effect of nanowire tension σ on the composite beam. Here we approximate the curved cantilever as a straight beam at angle θ. This allows straightforward calculation of the cantilever deflection δ due to loading by the nanowire tension. The angle θ is given by $\tan\theta = z_{\max}/l_c = \kappa l_c/2$, and the nanowire tension applies a load perpendicular to the beam of $\sigma\sin\theta$. The deflection of the composite beam is therefore

$$\delta = \frac{l_c^3 \sigma \sin\theta}{3K} \tag{S88}$$

The deflection of the cantilever end in the vertical direction is given by $\delta\cos\theta$. Thus we arrive finally at the change in vertical position per unit temperature change (i.e. stress change) of the nanowire:

$$D = \frac{d(\delta\cos\theta)}{dT} = \frac{l_c^3 \sin\theta \cos\theta}{3K} \frac{d\sigma}{dT} \tag{S89}$$

Because the bending stiffness (given by Eq. S86) $K \propto b$, where b is the cantilever width, this derivation reveals that the photothermal coupling $D \propto l_c^3/b$. This suggests that D can be drastically enhanced simply by using longer cantilevers. Moreover, the optimal cantilever angle is $\theta = 45°$.

S8. NOTE ABOUT GAUSSIAN BEAMS

Throughout this work we have, for the sake of simplicity, assumed a sinusoidal optical intensity profile $g(z)$ (see Eq. S3). Such a functional form is only approximately correct, as it presupposes optical plane waves of infinite breadth. In the more realistic case of an incident Gaussian laser beam, the functional form of $g(z)$ can deviate greatly from Eq. S3.

A Gaussian beam can be written as (Ref. 13)

$$U(x,y,z) = A_0 \frac{w_0}{w(z)} \exp\left[-\frac{x^2+y^2}{w^2(z)}\right] \exp\left[-ikz - ik\frac{x^2+y^2}{2R(z)} + i\zeta(z)\right] \tag{S90}$$

where $U(x,y,z)$ can denote either the electric or magnetic field; x, y, z are Cartesian coordinates with z lying along the beam axis (i.e. the direction of propagation). A_0 is the beam amplitude. Furthermore, we have

$$w(z) = w_0 \sqrt{1 + \left(\frac{z}{\Delta_z}\right)^2} \tag{S91}$$

$$R(z) = z\left[1 + \left(\frac{\Delta_z}{z}\right)^2\right] \tag{S92}$$

$$\zeta(z) = \tan^{-1}\frac{z}{\Delta_z} \tag{S93}$$

$$w_0 = \sqrt{\frac{\lambda\Delta_z}{\pi}} \tag{S94}$$

where $2\Delta_z$ is the depth-of-focus of the beam and $w_0 = d_L/2$ is the beam waist radius (i.e. spot size). The intensity at any point can be calculated from $I(x,y,z) = |U(x,y,z)|^2$, and the peak intensity of the beam (which occurs at $x = y = z = 0$) is $I_0 = |A_0|^2$. In terms of the total beam power P, we have $P = \frac{1}{2}I_0\pi w_0^2$.

Figure S6 shows the optical interference pattern generated (using Eq. S90) by a Gaussian beam normally incident on a perfect mirror with 100% reflectivity. The mirror is located at $z = 0$, and the beam waist is focused at $z/\lambda = 12$ (consistent with the nanowire location in our experiment). A black dot at $z/\lambda = 12$ in (a-c) is roughly the size of our nanowire cross-section. (a,b) show the incident and reflected beams, respectively, (real parts only) and (c) depicts the standing intensity profile produced by their interference. Note that this intensity is normalized to the incident beam intensity I_0 (or equivalently, A_0 has been set to 1 in Eq. S90). The intensity along the beam direction is plotted in (d) for three different values of x. The beam waist $w_0/\lambda = 1.26$ corresponds to a spot size of 1.6μm, roughly consistent with our experiment.

The curves in Fig. S6 (d) correspond to the true intensity profiles $g(z)$ for different x positions of our nanowire (neglecting effects of the nanowire itself, which are studied extensively in Ref. 14). Clearly our simple expression in Eq. S3 must therefore be updated to

$$g(z) = \alpha(z) + \beta(z)\sin^2\left(\frac{2\pi(z+\phi)}{\lambda} - \frac{\pi}{4} + \eta(z)\right) \tag{S95}$$

where α and β are now functions of z. Note that the added phase $\eta(z)$ is intended to account for $\zeta(z)$ in Eq. S90, which introduces a phase retardation of π as an unperturbed beam travels from $z = -\infty$ to $z = \infty$. Over typical experimental length-scales of $\lesssim \Delta_z$, however, this term can be neglected. Similarly, over typical oscillation amplitudes of $R \lesssim \lambda$, $\alpha(z)$ and $\beta(z)$ can be taken as constants. However, because $\alpha(z)$ and $\beta(z)$ depend strongly on the focused beam waist w_0, the distance of this focus from the mirror, and the nanowire's position in x, numerical values for these parameters are difficult to calculate and will likely vary slightly between successive measurements. As a rough approximation, data fitting throughout our main text was performed using $\alpha = 0.171$ and $\beta = 2.344$, values corresponding to a plane wave reflecting off of a Si mirror. Residuals between data and fits in Fig. 2 (c) of the main text can likely be reduced greatly by using linear expansions $\alpha(z) = \alpha_0 + \alpha_1 z$ and $\beta(z) = \beta_0 + \beta_1 z$, however doing so would add multiple fit parameters, negating the simplicity of the model used.
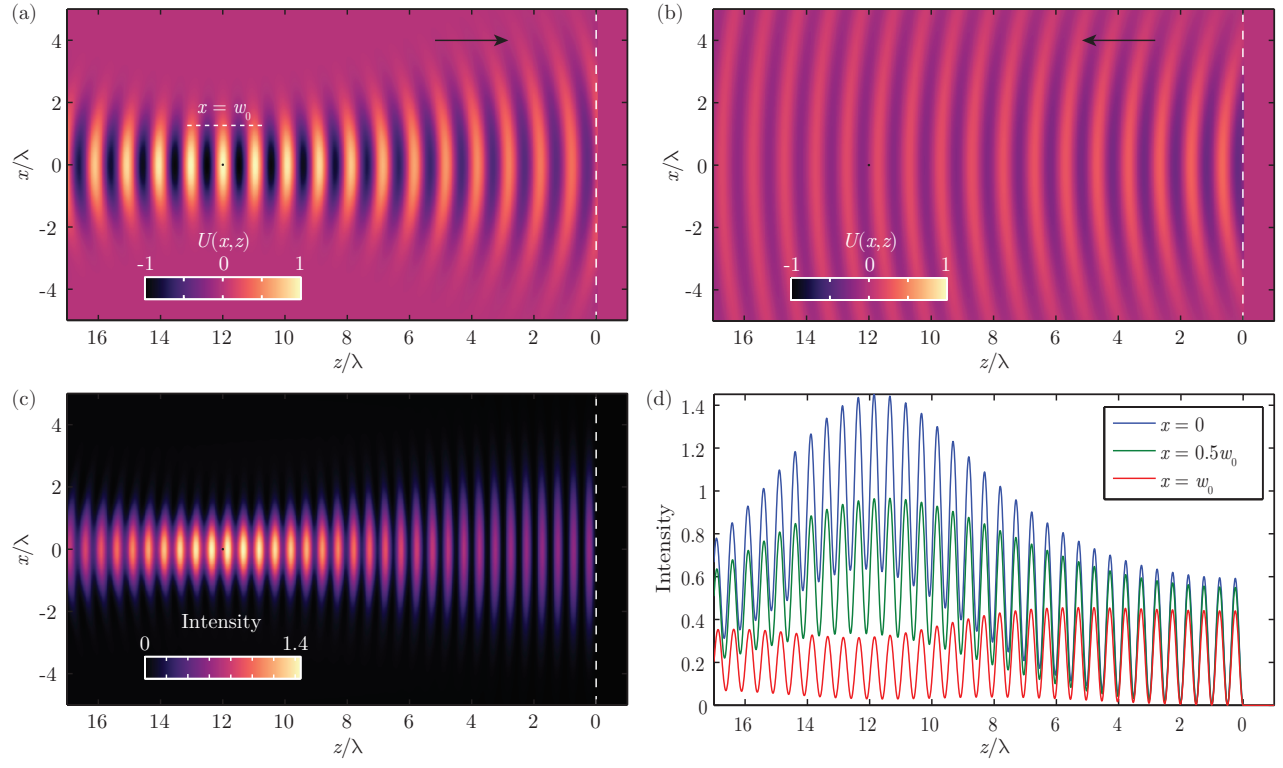
FIG. S6. Reflection of a Gaussian beam off of a perfect mirror.

S9.   NONLINEARITY OF THE OPTICAL READOUT TECHNIQUE

The motion of our nanowire is detected by measuring the intensity of laser light reflected from the sample. This reflection comes from the underlying Si back-plane, and is modulated by the absorption of our nanowire. We assume that the nanowire is sufficiently thin compared to the laser wavelength ($\lambda = 660\,\mathrm{nm}$) and spot size (Gaussian beam diameter $d_L \approx 2\,\mu\mathrm{m}$) that it does not cause significant reflections itself or trap any light between the nanowire and mirror as in an optical cavity. Indeed, the $\sim 50\,\mathrm{nm}$-wide nanowire acts as a single slit causing any reflected laser light to diffract away from the optical axis quite rapidly.

The power measured by our high-speed photo-detector can be approximated by $P - P_{\mathrm{loss}} - P_{\mathrm{abs}}(z)$, where P is the incident laser power, P_{loss} is the power absorbed by the mirror, and $P_{\mathrm{abs}}(z)$ is the position-dependent power absorbed by our nanowire. As shown in Eq. S79, the absorbed power is

$$P_{\mathrm{abs}}(z) = aPg(z) \tag{S96}$$

where a describes the absorptive properties of the Nb film on our nanowire. The dimensionless optical intensity profile $g(z)$ (reproduced form Eq. S3) is:

$$g(z) = \alpha - \beta \sin\left(\frac{4\pi(z + \phi)}{\lambda}\right) \tag{S97}$$

where α, β are constants, ϕ is the nanowire's initial location within the optical field. The voltage generated by our photo-detector is therefore

$$V(t) = bGP[1 - ag(z(t))] \tag{S98}$$

where b denotes any optical losses between the nanowire and the photo-detector (e.g. reflections at air-lens interfaces), and G is the photo-detector gain.

The nonlinear relationship between $z(t)$ and $V(t)$ generates harmonics of the nanowire oscillation frequency ω in the detected voltage. The strength of these harmonics can be calculated in an analogous fashion to the terms $(V_1, V_2, \cdots)$ in Section S1. To do this, the nanowire motion is again modeled by $z = x + z_0$, where $x = R\cos\omega t$ describes the oscillation (with amplitude R and frequency ω) and z_0 is the equilibrium position.

If the optical field $g(x + z_0)$ is approximated by an Nth order polynomial (see Eq. S10) $h(x) \approx g(x + z_0)$, then the voltage detected at frequency $n\omega$ (where n is a positive integer) has amplitude

$$V_{n\omega} = -2abGP \sum_{m=0}^{M_n} \frac{h_0^{(2m+n)}}{m!(m+n)!} \left(\frac{R}{2}\right)^{2m+n} \tag{S99}$$

Here $h_0^{(n)}$ is the nth derivative of $h(x)$ evaluated at $x = 0$ or, equivalently, the nth derivative of $g(z)$ evaluated at $z = z_0$. The summation above terminates at $M_n = \mathrm{floor}((N - n)/2)$, where N is again the polynomial order or $h(x)$. See Eqs. S26 - S31 for details on the derivation.

If we take $N = 7$, the first three harmonics are given by:

$$V_{1\omega} = -2abGP \left[\frac{h_0^{(1)}}{0!1!}\left(\frac{R}{2}\right) + \frac{h_0^{(3)}}{1!2!}\left(\frac{R}{2}\right)^3 + \frac{h_0^{(5)}}{2!3!}\left(\frac{R}{2}\right)^5 + \frac{h_0^{(7)}}{3!4!}\left(\frac{R}{2}\right)^7 \right] \tag{S100}$$

$$V_{2\omega} = -2abGP \left[\frac{h_0^{(2)}}{0!2!}\left(\frac{R}{2}\right)^2 + \frac{h_0^{(4)}}{1!3!}\left(\frac{R}{2}\right)^4 + \frac{h_0^{(6)}}{2!4!}\left(\frac{R}{2}\right)^6 \right] \tag{S101}$$

$$V_{3\omega} = -2abGP \left[\frac{h_0^{(3)}}{0!3!}\left(\frac{R}{2}\right)^3 + \frac{h_0^{(5)}}{1!4!}\left(\frac{R}{2}\right)^5 + \frac{h_0^{(7)}}{2!5!}\left(\frac{R}{2}\right)^7 \right] \tag{S102}$$

The derivatives $h_0^{(n)}$ are listed in Eq. S25. Note that the odd harmonics of V only contain odd derivatives of $h(x)$ while the even harmonics only contain even derivatives. This suggests that odd harmonics of V vanish when z_0 is located at an extremum in $g(x + z_0)$, while even harmonics vanish when z_0 is at an inflection point in $g(x + z_0)$. Also note that for low laser powers, when the nanowire is not undergoing self-oscillation, small-amplitude motion $R \ll \lambda$ results in the linear relationship $V_{1\omega} \approx -abGPh_0^{(1)}R$ and $V_{2\omega} \approx V_{3\omega} \approx 0$. This linear relation between the vibration amplitude R and detected voltage $V_{1\omega}$ allows us to measure Lorentzian lineshapes upon driving nanowire motion inertially, as is shown in Fig. 1 (c) of the main text.

REFERENCES

[1] R. Rand, *Lecture Notes on Nonlinear Vibrations* (Cornell University, Ithaca, NY, 2012).

[2] A. M. Lyapunov, International Journal of Control **55**, 531 (1992).

[3] D. Southworth, R. Barton, S. Verbridge, B. Ilic, A. Fefferman, H. Craighead, and J. Parpia, Physical Review Letters **102**, 225503 (2009).

[4] M. Poot, S. Etaki, I. Mahboob, K. Onomitsu, H. Yamaguchi, Y. M. Blanter, and H. S. J. van der Zant, Physical Review Letters **105**, 207203 (2010).

[5] S. Etaki, F. Konschelle, Y. M. Blanter, H. Yamaguchi, and H. S. J. van der Zant, Nature Communications **4**, 1803 (2013).

[6] J. V. Porto and J. M. Parpia, Physical Review B **59**, 14583 (1999).

[7] D. Aspnes and A. Studna, Physical Review B **27**, 985 (1983).

[8] MIT Material Properties Database, `www.mit.edu/~6.777/matprops/matprops.htm`w (2017).

[9] M. Winter, WebElements: `www.webelements.com` (2017).

[10] T. Tokuyama, Y. Fujii, Y. Sugita, and S. Kishino, Japanese Journal of Applied Physics **6**, 1252 (1967).

[11] A. Golovashkin, I. Leksina, G. Motulevich, and A. Shubin, Soviet Physics JETP **29**, 27 (1969).

[12] W.-H. Chu, M. Mehregany, and R. L. Mullen, Journal of Micromechanics and Microengineering **3**, 4 (1993).

[13] B. E. A. Saleh and M. C. Teich, *Fundamentals of Photonics*, 2nd ed. (Wiley-Interscience, 2007).

[14] D. Ramos, E. Gil-Santos, V. Pini, J. M. Llorens, M. Fernández-Regúlez, Á. San Paulo, M. Calleja, and J. Tamayo, Nano Letters **12**, 932 (2012).